Journal of Materials Chemistry A

PAPER

View Article Online
View Journal | View Issue

Cite this: J. Mater. Chem. A, 2014, 2, 3452

High performance of Pt-free dye-sensitized solar cells based on two-step electropolymerized polyaniline counter electrodes

Yaoming Xiao,* Gaoyi Han,* Yanping Li, Miaoyu Li and Yunzhen Chang

Received 25th November 2013
Accepted 7th December 2013

DOI: 10.1039/c3ta14879c

www.rsc.org/MaterialsA

A two-step cyclic voltammetry (CV) approach is employed in a quick and controllable electropolymerization of polyaniline (PANI) nanofibers with a short-branched structure onto fluorinated tin oxide (FTO) glass substrates as counter electrodes (CEs) for Pt-free dye-sensitized solar cells (DSSCs). In the two-step CV method, a small quantity of PANI as a function of the crystal nucleus in the crystal growth, is pre-electropolymerized under a suitably high potential for one cycle at the first-step, then subjected to the second-step for PANI electropolymerization at a low potential for a small number of scans. The well-controlled PANI nanofibers with high performance can be electropolymerized quickly using the two-step mode. The extensive CVs demonstrate the two-step PANI CE has superior electrocatalytic activity for the I_3^- reduction. Moreover, electrochemical impedance spectroscopy shows that the two-step PANI CE has a lower series resistance and charge-transfer resistance than the PANI CE prepared by conventional one-step CV electropolymerization. Therefore, the DSSC assembled with the two-step PANI CE exhibits an enhanced photovoltaic conversion efficiency of 6.21% (compared to 5.01% for the DSSC with the one-step PANI CE), up to ~97% of the level of the DSSC using Pt CE. As the result, the two-step CV electropolymerized PANI CE can be considered as a promising alternative CE for Pt-free DSSCs.

Introduction

Dye-sensitized solar cells (DSSCs) have attracted the scientific and technological interest of researchers in the past decades as a high efficiency and low-cost alternative to conventional silicon p–n junction photovoltaic devices.[1–3] In general, the DSSC consists of a dye-sensitized porous nanocrystalline TiO_2 electrode, a iodine-based electrolyte, and platinum (Pt) as a counter electrode (CE).[4,5] The function of the CE is to transfer electrons from the external circuit back to the redox electrolyte and to catalyze the reduction of I_3^- to I^-. However, Pt metal is one of the most expensive component materials in DSSCs.[2,5] In addition, the Pt can be decomposed to PtI_4 in a traditional I^-/I_3^- redox couple electrolyte, which will affect the long-term stability of the DSSC.[6] Thus, it is necessary to develop an economic, stable, effective and Pt-free CE to realize large-scale industrialization of DSSCs.[7,8] As such, a great deal of materials, such as carbon-based materials,[9–12] sulfides,[13–15] nitrides,[16,17] and conducting polymers,[18–21] have been suggested to replace the Pt CE.

Among them, conducting polymers have been used in the polymer gel electrolyte[22–25] and CEs in DSSCs, and polyaniline (PANI) is one of the most promising conducting polymers to be employed as a cost-effective Pt-free CE for catalyzing the I_3^- reduction reaction in DSSCs, due to its low cost, high electrochemical activity and environmental stability.[18,26–32] It is well known that PANI can be easily synthesized through chemical polymerization[18] and electropolymerization methods.[26–32] The latter set of methods is a considerably simpler and more cost-effective technique to obtain conducting polymers with controllable surface morphology and good adhesion on the substrate surface. The reported electropolymerization methods used in synthesizing PANI include: cyclic voltammetry (CV),[26,27] constant potential,[28,29] constant current,[30] pulse current[31] and pulse potentiostatic[32] methods.

In our preliminary experiments, we found that it was hard to synthesize PANI by using conventional CV methods at low potential even for large number of scans, and it was too fast and uncontrollable at high potentials for a small number of scans (as shown in Fig. 1a–d and h). Therefore, we report a new approach, named the two-step CV method (as shown in Fig. 1e–g), to realize the quick and well-controlled electropolymerization of PANI nanofibers onto fluorinated tin oxide (FTO) glass substrates as CEs for Pt-free DSSCs in this study. Basically, a small quantity of PANI, as a function of the crystal nucleus in the crystal growth, was pre-electropolymerized under a suitable high potential for one cycle at the first-step, then subjected to the second-step for PANI electropolymerization at a low potential for small number of scans. The obtained PANI CE demonstrated superior electrocatalytic activity for I_3^- reduction, and showed lower series resistance and charge-transfer

Institute of Molecular Science, Key Laboratory of Chemical Biology and Molecular Engineering of Education Ministry, Shanxi University, Taiyuan 030006, P. R. China. E-mail: ymxiao2011@sohu.com; han_gaoyis@sxu.edu.cn; Fax: +86 351 7016358; Tel: +86 351 7010699

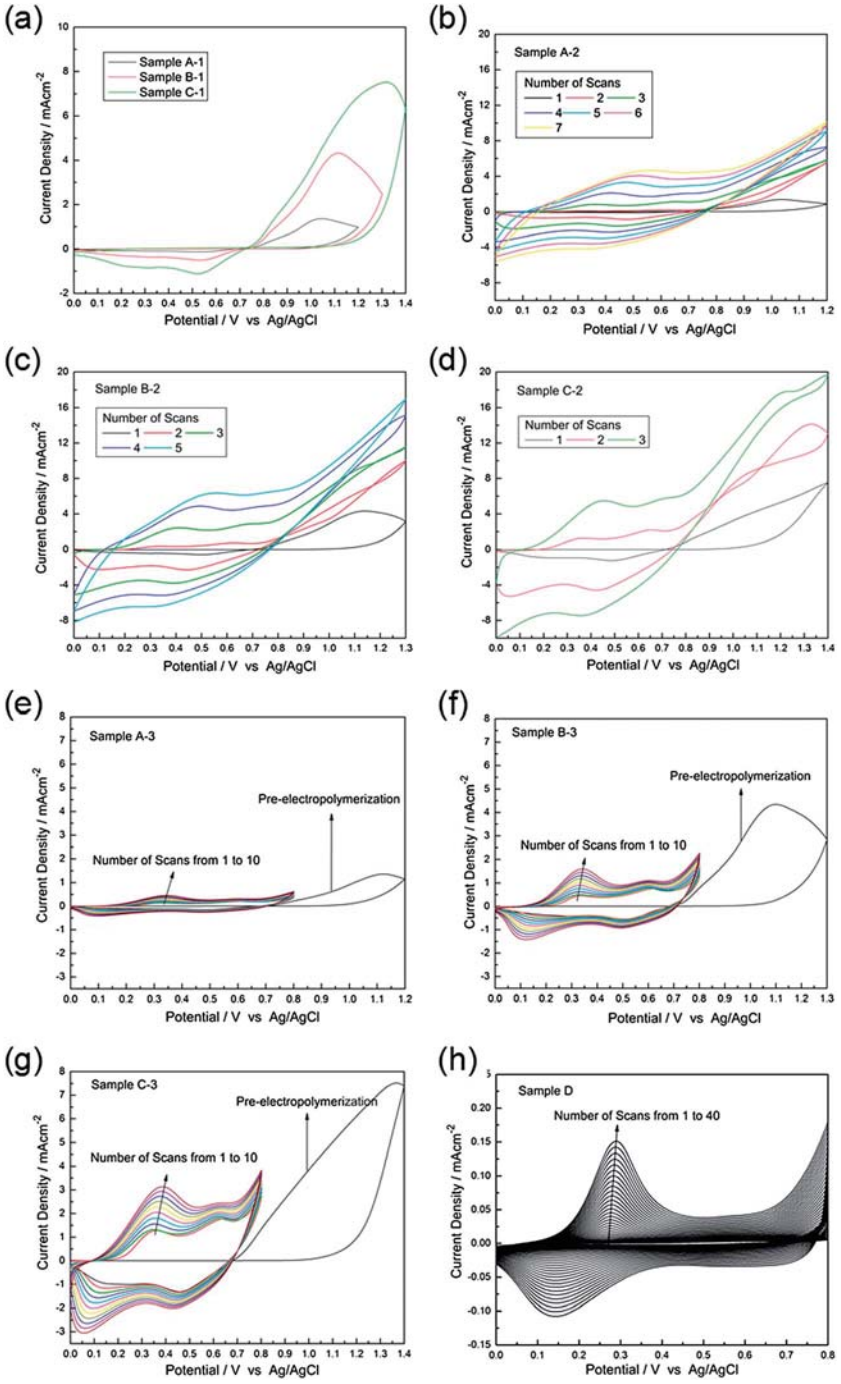

Fig. 1 CV electrodeposition of PANI CEs on FTO glasses with each active area of 1.0 cm × 1.5 cm.

resistance than PANI CE prepared by the conventional one-step CV electropolymerization. The DSSC assembled with the two-step PANI CE exhibited a photovoltaic conversion of 6.21% superior to that of the DSSC with a conventional one-step PANI CE, and was comparable to that of a cell with a Pt CE.

Experimental

Materials

Aniline monomer, sulfuric acid, acetone, ethanol, isopropyl alcohol, lithium perchlorate, iodine, lithium iodide, tetrabutyl ammonium iodide, 4-*tert*-butyl-pyridine and acetonitrile were purchased from Shanghai Chemical Agent Ltd., China (Analysis purity grade). Sensitized-dye N719 [*cis*-di(thiocyanato)-*N*,*N*′-bis(2,2′-bipyridyl-4-carboxylic acid-4-tetrabutylammonium carboxylate) ruthenium(II)] was purchased from Dyesol, Australia. The above agents were used without further purification.

Electropolymerization of PANI CEs

All the PANI films were electropolymerized on the FTO glass substrates (NSG, 13 Ω sq^{-1}) from an aqueous solution

containing 0.5 M aniline monomer and 0.5 M sulfuric acid in a three compartment cell. Prior to electropolymerization, FTO substrates (1.5 cm × 2 cm) were cleaned with acetone and isopropyl alcohol, respectively. A Pt wire, a saturated silver/silver chloride (Ag/AgCl) and a cleaned FTO glass substrate were used as the counter electrode, the reference electrode and the working electrode, respectively.

The CV electropolymerization of PANI was carried out using a computer-controlled Autolab potentiostat (PGSTAT320N) at ambient atmosphere. The parameters for PANI CEs were listed in Table 1. In brief, one-step CV electropolymerization was conducted under one potential interval range, and two-step CV was controlled at two different potential ranges. Under the two-step CV electropolymerization, for example, the potential range was firstly set between 0 V and 1.3 V for 1 cycle for the pre-electropolymerization and then subjected to the second-step for the PANI electropolymerization between 0 V and 0.8 V for 10 cycles *vs.* Ag/AgCl at a scan rate of 0.05 V s^{-1}. The obtained CEs were designated as Sample A-1, B-1, C-1, and so on, which correspond to Table 1. The achieved PANI CE was rinsed in distilled water and dried under a cool air flow. For comparison, a thermal decomposition Pt CE was employed.

Characterizations and measurements

The surface morphologies of the PANI CEs were observed using a scanning electron microscope (SEM, JEOL-JSM-6701F) operating at 10 kV and a transmission electron microscope (TEM, JEOL-JSM-2100) operating at 200 kV. Fourier transform infrared spectra (FTIR) of the samples were recorded on an Infrared Spectrometric Analyzer (BRUKER TENSOR 27) using KBr as pellets. CVs for the I^-/I_3^- system (solution of 10 mM lithium iodide, 1 mM iodine, and 0.1 M lithium perchlorate in acetonitrile) were conducted using the aforementioned Autolab potentiostat within the potential interval ranging from −0.6 V to 1.2 V *vs.* Pt at a scan rate of 0.10 V s^{-1}. Electrochemical impedance spectroscopy (EIS) was performed using a CHI660D (Shanghai Chenhua Device Company, China) electrochemical measurement system at a constant temperature of 20 °C in ambient atmosphere under dark conditions, and the impedance data covered a frequency range of 1 to 10^5 Hz with 5 mV of amplitude and zero bias potential. The detailed produce for the fabrication of the symmetric dummy cell with two identical electrodes (used for impedance studies) has been reported elsewhere.[33,34] The resultant impedance spectra were simulated using Z-view software. The redox electrolyte composed of 0.60 M tetrabutyl ammonium iodide, 0.10 M lithium iodide, 0.10 M iodine, and 0.50 M 4-*tert*-butyl-pyridine in acetonitrile was employed in EIS measurements.

The photocurrent density–voltage characteristic of the DSSC was carried out using a computer-controlled CHI660D under illumination by a solar simulator (CEL-S500, Beijing CeAuLight Science and Technology Ltd., China) in an ambient atmosphere. The active cell area and the incident light intensity were 0.30 cm^2 and 100 mW cm^{-2} (AM 1.5), respectively. Prior to the cell assembly, the TiO_2 colloid and TiO_2 photoanodes were prepared according to our previous reports.[7,35] The as-prepared TiO_2 photoanodes were further sensitized by immersing them into a 0.3 mM ethanol solution composed of N719 dye for 12 h, followed by cool air drying. After dye adsorption, the TiO_2 photoanodes were assembled with Pt and various PANI CEs. Then the redox electrolyte (aforementioned EIS testing electrolyte) was injected into the cells. The photoelectronic performances [*i.e.*, fill factor (FF) and overall energy conversion efficiency (η)] were calculated by the following equations:[36]

$$\mathrm{FF} = \frac{V_{\max} \times J_{\max}}{V_{\mathrm{oc}} \times J_{\mathrm{sc}}} \quad (1)$$

$$\eta(\%) = \frac{V_{\max} \times J_{\max}}{P_{\mathrm{in}}} \times 100\% = \frac{V_{\mathrm{oc}} \times J_{\mathrm{sc}} \times \mathrm{FF}}{P_{\mathrm{in}}} \times 100\% \quad (2)$$

where J_{SC} is the short-circuit current density (mA cm^{-2}), V_{OC} is the open-circuit voltage (V), P_{in} is the incident light power, J_{max} (mA cm^{-2}) and V_{max} (V) are the current density and voltage in the *J–V* curves at the point of maximum power output, respectively.

Table 1 Parameters of CV electropolymerization for the various PANI CEs

Samples	Scan rate/ V s^{-1}	Start potential/V	First vertex potential/V	Second vertex potential/V	Number of scans	Deposition capacities/mC cm^{-2}	
						Q_+	Q_-
A-1	0.05	0	0	1.2	1	9.08	−1.19
B-1	0.05	0	0	1.3	1	37.39	−5.42
C-1	0.05	0	0	1.4	1	80.68	−11.94
A-2	0.05	0	0	1.2	7	26.87	−8.11
B-2	0.05	0	0	1.3	5	158.91	−55.83
C-2	0.05	0	0	1.4	3	266.20	−69.35
A-3	0.05	0	0	1.2	1	9.13	−1.21
	0.05	0	0	0.8	10	6.76	−4.84
B-3	0.05	0	0	1.3	1	39.63	−5.87
	0.05	0	0	0.8	10	18.13	−12.98
C-3	0.05	0	0	1.4	1	81.46	−12.58
	0.05	0	0	0.8	10	42.88	−32.80
D	0.05	0	0	0.8	40	1.08	−0.87

Results and discussion

Electrochemical synthesis of PANI CEs

Fig. 1 shows the CV electropolymerization of PANI CEs based on different parameters, and the deposition capacities were listed in Table 1. It can be seen that the current density increases distinctly after the Second Vertex Potential of about 1.05 V at the first CV cycle of each sample (Fig. 1a Sample A-1, or B-1, or C-1), suggesting the PANI was barely electrodeposited on the FTO glass before the potential of 1.05 V. The current density and deposition capacity increase with the enlargement of the Second Vertex Potential (Fig. 1a), implying that more and more PANI was electropolymerized on the FTO glass with the higher potential. According to Fig. 1b–d, the current density and deposition capacity increase significantly with adding to the number of scans in each sample, and the higher the Second Vertex Potential, the larger the rate of increase within a lesser number of scans. As can be seen in Fig. 1h, when the potential range was set between 0 V and 0.8 V, the current density and deposition capacity are very low, even when deposited for 40 cycles, meaning that barely no PANI was produced.

Fig. 1e–g demonstrate two-step CV electropolymerization of PANI CEs based on different pre-electropolymerization potential interval ranges at the first-step and the same second-step potential range for the PANI electropolymerization. It is interesting that even when the second-step potential range was set between 0 V and 0.8 V for 10 cycles, the current density and deposition capacity obviously improved after the first-step pre-electropolymerization of PANI, meaning that the PANI was successfully prepared on the FTO glass. And the higher the Second Vertex Potential in the first-step pre-electropolymerization, the larger the current density and deposition capacity in the second-step electropolymerization of the PANI.

Morphology and composition of PANI CEs

The SEM images of various PANI CEs are shown in Fig. 2. It can be found that more and more PANI nanofibers are generated with increasing Second Vertex Potential (Fig. 2A-1, B-1 and C-1). Under the one-step approach, it is hard to synthesize PANI at the low Second Vertex Potential even for a large number of scans (Fig. 2D). Moreover, it is too fast and uncontrollable to prepare PANI at the high Second Vertex Potential for a smaller number of scans (Fig. 2A-2, B-2 and C-2). It can be noted that the surface of PANI nanofibers became uniform when the electropolymerization method was switched from the one-step mode to the two-step mode (Fig. 2A-3, B-3 and C-3). The last three digital photograph images in Fig. 2 correspond to the real pictures of the Sample B-1, B-2 and B-3, respectively. There is too small a number of PANIs in the Sample B-1, a nonuniform and uncontrollable surface in Sample B-2, and well-controlled PANI nanofibers with a uniform surface in Sample B-3. It should be noted that the electropolymerization time was sharply cut down by using the two-step CV approach.

Fig. 3 shows the higher magnification of SEM and TEM images to investigate further the structures of the Samples B-1, B-2 and B-3, respectively. It can be found that a small number of short and smooth PANI nanofibers with a diameter of 30–60 nm and a length of about 400 nm were pre-electropolymerized in the Sample B-1 (Fig. 3B-1-1–B-1-3). In the one-step mode, agglomerated and rough PANI nanofibers with a diameter of 50–100 nm and a length of about 500 nm, can be observed in the Sample B-2 (Fig. 3B-2-1–B-2-3). Under the two-step mode, well-controlled PANI nanofibers with a uniform and short-branched structure could be obtained in Sample B-3 (Fig. 3B-3-1–B-3-3), and short-branched PANIs with a diameter of 10–20 nm and a length of 40–80 nm were electropolymerized on the pre-electropolymerized PANI nanofibers. The possible mechanism could be that a small quantity of PANI nanofibers, was pre-electropolymerized under a suitably high potential at the first-step, then the second-step would be the rapid and successful electropolymerization of short-branched PANIs at a low potential; due to the first-step pre-electropolymerized PANIs could act as the function of crystal nucleus in the crystal growth. After optimization, the PANI CE prepared in the potential range between 0 V and 1.3 V for 1 cycle for the first-step pre-electropolymerization and then subjected to the second-step electropolymerization between 0 V and 0.8 V for 10 cycles possessed the unique characteristics of well-controlled PANI nanofibers with a short-branched morphology on the FTO substrate. It can be envisaged that the well-controlled PANI nanofibers could establish an excellent electron transport network and the short-branched PANIs could increase the active surface area, thus being expected to enhance the electrocatalytic activity for PANI-based CEs.

To characterize the composition of the electropolymerised PANI CEs, the PANI was collected together from the FTO glass, and the FTIR spectra of the B-1, B-2 and B-3 PANIs were performed. As shown in Fig. 4, the spectra for the three types of PANI look almost the same. The contribution from C–H bending of the quinoid ring appears at 1120 and 1144 cm^{-1}. The C–N bending mode and stretching mode are also observed at 1246 and 1305 cm^{-1}, respectively. The characteristic absorption signals of the PANI nanofiber, appearing at 1501 and 1586 cm^{-1}, can be attributed to the benzenoid deformation and C=C stretching of the quinoid ring of PANI, respectively.[32,37] The FTIR spectra indicate that the PANI nanofibers were successfully deposited onto the surfaces of FTO glass substrates.

Electrochemical properties of PANI CEs

Fig. 5a shows CVs for the Pt, B-1, B-2 and B-3 PANI CEs, respectively. The CEs all show two pairs of redox peaks. The oxidation and reduction pair on the left is attributed to the redox reaction of $I_3^- + 2e^- \leftrightarrow 3I^-$, which directly affects the DSSC performance; while that on the right results from the redox reaction of $3I_2 + 2e^- \leftrightarrow 2I_3^-$, which has little effect on the DSSC performance.[7,33,38,39] It can be seen that the B-3 PANI CE shows the largest anodic and cathodic current densities for I_3^-/I^- redox reaction among these four CEs, which can be attributed its short-branched structure of the PANI nanofibres with a high active surface area, as demonstrated in the TEM results. Notably, the B-1 PANI shows the lowest redox current density, as the smallest number of PANI was grown on the FTO glass under the Second Vertex Potential of 1.2 V for only 1 cycle.

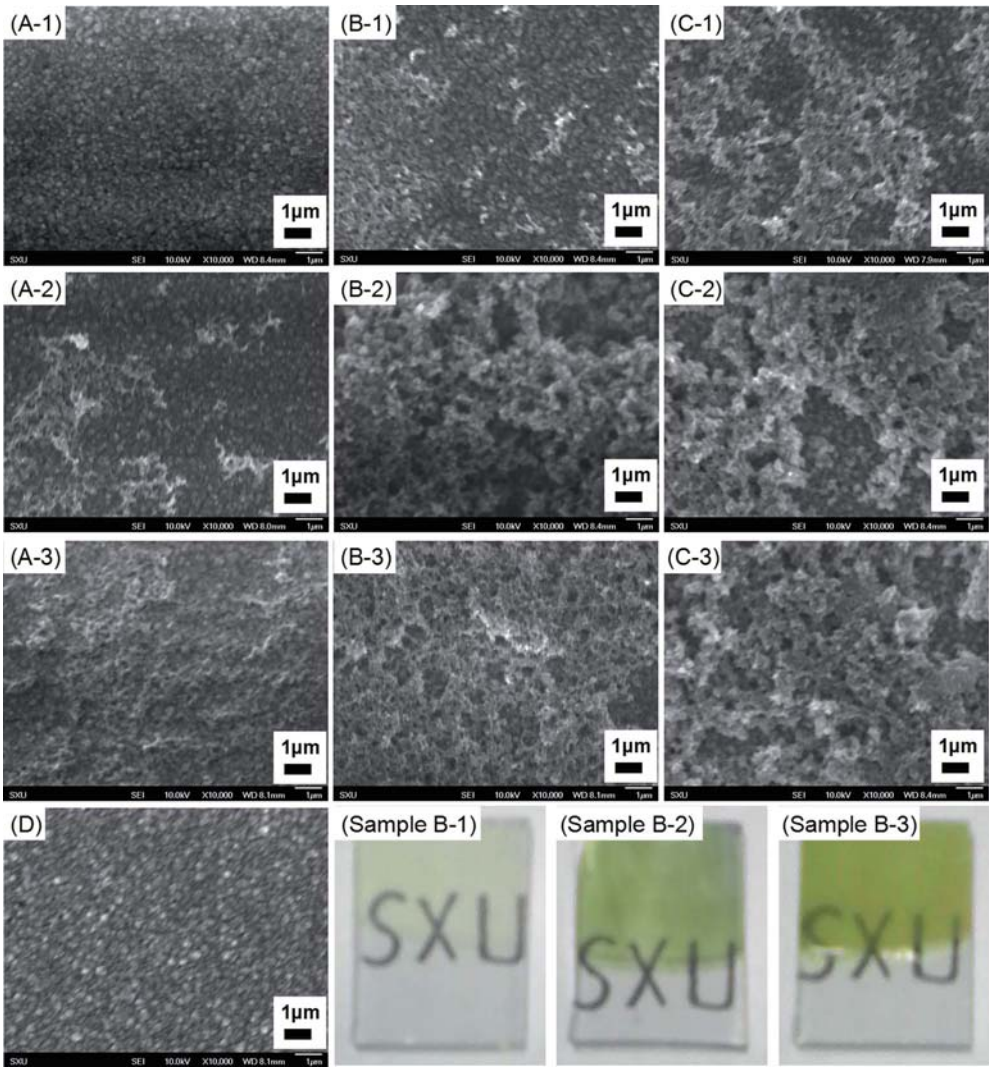

Fig. 2 SEM images of various PANI CEs based on Sample A-1, B-1, C-1, A-2, B-2, C-2, A-3, B-3, C-3 and D, respectively; and digital photographs of PANI CEs based on Sample B-1, B-2 and B-3, respectively.

Fig. 5b–e show CVs of the I_3^-/I^- system on the Pt, B-1, B-2 and B-3 PANI CEs at various scan rates, respectively. For these four CEs, the cathodic peaks gradually and regularly shifted negatively, and the corresponding anodic peaks also shifted positively while increasing scan rate. Fig. 5f illustrates the relationship between the cathodic and anodic peak current densities and the square root of the scan rate. The linear relationship at different scan rates demonstrates that this redox reaction is diffusion-limited at either the Pt CE or PANI CE, which may be due to the transport of iodide species off the Pt or PANI CE surface.[40,41] This suggests that the adsorption of iodide species is little influenced by the redox reaction on the both CEs' surface, thus indicating no specific interaction between the I_3^-/I^- redox couple and PANI CE as well as the Pt CE.[40]

In addition, the diffusion coefficient (D_n) in the Randles–Sevcik equation can be estimated from the correlation between the peak current density (J_{red}) and scan rate (v), as illustrated in eqn (3).

$$J_{red} = Kn^{1.5}AC(D_n)^{0.5}v^{0.5} \quad (3)$$

where K is the constant of 2.69×10^5, n is the number of electrodes contributing the charge transfer, A is electrode area, and C represents the bulk concentration of I_3^- species. As listed in Table 2, the diffusivity with the B-3 PANI CE was 4.76×10^{-6} $cm^{-2}\ s^{-1}$, which was larger than that with the B-1 PANI CE ($1.55 \times 10^{-9}\ cm^{-2}\ s^{-1}$), B-2 PANI CE ($1.46 \times 10^{-6}\ cm^{-2}\ s^{-1}$) and the Pt CE ($2.28 \times 10^{-6}\ cm^{-2}\ s^{-1}$), presumably originating from its well-controlled surface structure.[42]

Furthermore, Fig. 6a shows 160 consecutive CV tests of the B-3 PANI CE. In the successive 160 CV cycles, the CVs do not change. The correlations between the peak current densities and the cycle numbers were summarized in Fig. 6b. Both redox peak current densities retain stable with increasing cycle number. This proves that the B-3 PANI has good chemical stability and is tightly bound to the FTO glass surface.[43]

As the charge-transfer resistance (R_{ct}) is an index to represent the electrocatalytic performance of CEs, Nyquist plots (Fig. 7)

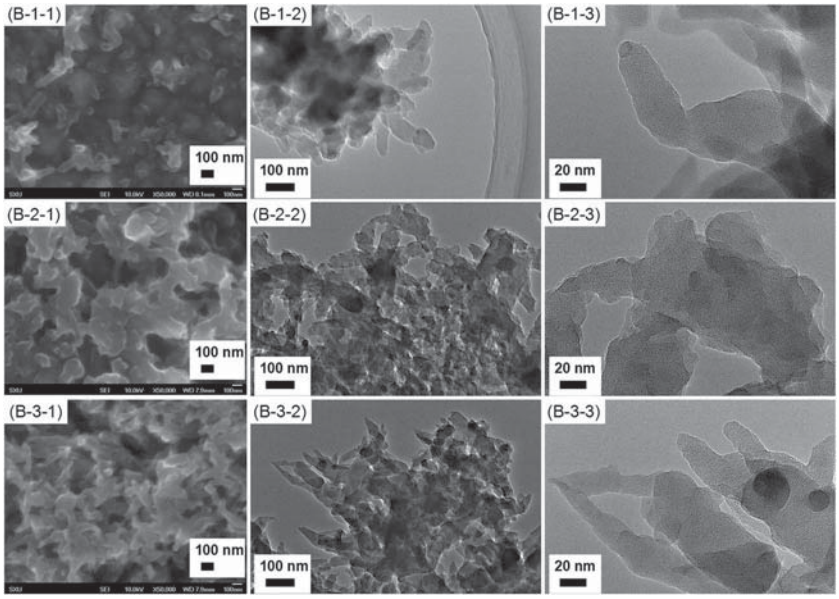

Fig. 3 SEM images of the B-1 (B-1-1), B-2 (B-2-1) and B-3 (B-3-1) PANI CEs, respectively; and TEM images of various PANIs based on Sample B-1 (B-1-2 and B-1-3), B-2 (B-2-2 and B-2-3) and B-3 (B-3-2 and B-3-3), respectively.

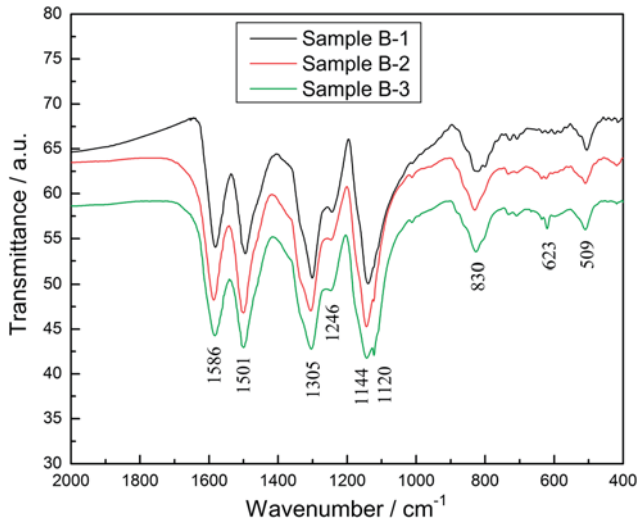

Fig. 4 FTIR spectra of the PANI based on Sample B-1, Sample B-2 and Sample B-3, respectively.

were measured to elucidate further the electrochemical catalysis of different CEs on the reduction of I_3^-, by using symmetrical cells with the Pt, B-1, B-2 and B-3 PANI CEs, respectively. Insets of Fig. 7 illustrate the electrochemical cell for the EIS measurement, the equivalent circuit models employed to simulate the resultant spectra of CEs and the magnification of the Nyquist plots. The semicircle at high frequency refers to the R_{ct} of the I_3^- reduction at the electrolyte/CE interface, while the semicircle at low frequency represents the Warburg impedance (W) corresponding to the diffusion resistance of the I^-/I_3^- redox species. The constant phase element (CPE) is frequently used as a substitute for the capacitor in an equivalent circuit to fit the impedance behavior of the electrical double layer more accurately when the double layer does not behave as an ideal capacitor. The intercept of the real axis at high frequency is the ohmic series resistance (R_S) including the sheet resistance of two identical CEs and the electrolytic resistance.[44]

Table 2 shows the impedance parameters obtained from the Z-view software analyses of the EIS data. Due to the symmetric configuration of the dummy cell, the real R_{ct} value was calculated as half of the value obtained from the Z-view fitting. The R_{ct} of the B-3 PANI CE is found to be 2.16 Ω cm^2, which is lower than that of the B-1 PANI CE (7.83 Ω cm^2) and the B-2 PANI CE (2.51 Ω cm^2). This indicates that the electrocatalytic activity for I_3^- reduction can be enhanced when the electropolymerization mode is switched from the one-step method to the two-step approach.[45–47] Additionally, the largest CPE magnitude (Y_{CPE} = 1.75 mF cm^{-2}) of the B-3 PANI CE corresponds to its short-branched structure with large surface area, which can promote the electrocatalytic activity of the PANI CE. This is consistent with CV tests. Furthermore, the B-3 PANI CE had the lowest W (2.12 Ω cm^2) compared to the other three CEs.

Photovoltaic performance of DSSCs with Pt and various PANI CEs

The photovoltaic properties of DSSCs based on different CEs were measured under full sunlight illumination (100 mW cm^{-2}, AM1.5 G) (upper curves) and in the dark (lower curves), which were reproduced many times without obvious change, and the results were summarized in Table 3. As can be seen in Fig. 8 (upper curves), the short-circuit current density (J_{SC}) value of the B-3 PANI CE was highest among all CEs; this might be due to the higher electrocatalytic active area of its well-controlled and short-branched nanofibers, as indicated in the TEM and CV tests.[7,40] Generally, the V_{OC} value depends on the difference between the Fermi level of the electron in TiO_2 and the cathodic

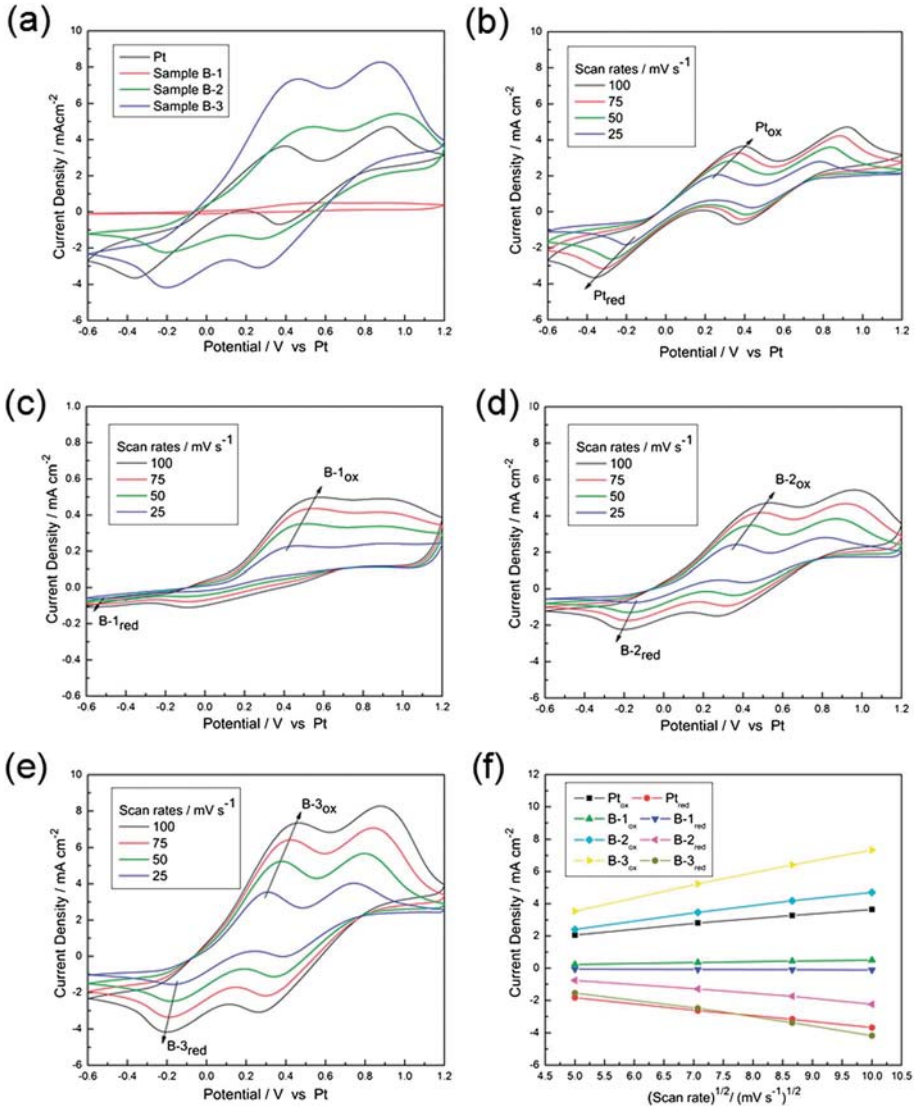

Fig. 5 CVs (a) of the Pt, B-1, B-2 and B-3 PANI CEs at a scan rate of 100 mV s^{-1}, respectively; CVs for the Pt (b), B-1 (c), B-2 (d) and B-3 (e) PANI CEs at different scan rates (from inner to outer: 25, 50, 75 and 100 mV s^{-1}, respectively); relationship (f) between all the redox peak currents and scan rates.

Table 2 Best-fit values of R_S, R_{ct}, W and Y_{CPE} in the equivalent circuits used to simulate the impedance spectra in Fig. 7; and the diffusion coefficients (D_n) based on the Pt, B-1, B-2 and B-3 PANI CEs, respectively

Samples	R_S/Ω cm^2	R_{ct}/ Ω cm^2	W/Ω cm^2	Y_{CPE}/ mF cm^{-2}	D_n/cm^{-2} s^{-1}
Pt	9.06	1.48	2.51	0.29	2.28×10^{-6}
B-1	10.54	7.83	260.24	0.01	1.55×10^{-9}
B-2	10.08	2.51	31.89	0.62	1.46×10^{-6}
B-3	9.69	2.16	2.12	1.75	4.76×10^{-6}

potential of the redox couples on the CEs.[1] Because the TiO_2 photoanodes and the compositions of the electrolytes for all of the DSSCs are the same, the V_{OC} value of each DSSC is associated with the electrochemical characteristics of the CE. It can be seen that the V_{OC} values of the PANI-based DSSCs are lower than that of the Pt DSSC. However, due to their high electrochemical activities, the DSSCs with the PANI-based CEs still possess relatively high V_{OC} values (~0.72 V), comparable to that of the Pt CE (0.75 V). Fig. 8 (lower curves) also shows the dark current–voltage characteristics of the corresponding photocurrent–voltage curves. It is obvious that the voltages of the DSSCs with the PANI-based CEs are lower than that of the Pt CE, which indicates that the internal consumptions of current are higher than that of the Pt CE, leading to the low open-circuit voltages.[48] Moreover, the overall performance of the DSSC assembled with the B-3 PANI CE is superior to that of the B-1 PANI CE and B-2 PANI CE, and exhibits an acceptable fill factor (FF) value of 0.59, supplying a cell efficiency of 6.21% comparable to those of a cell with a Pt CE (0.63 and 6.39%). This can be attributed to its higher R_S and R_{ct} values (9.69 and 2.16 Ω cm^2, respectively),

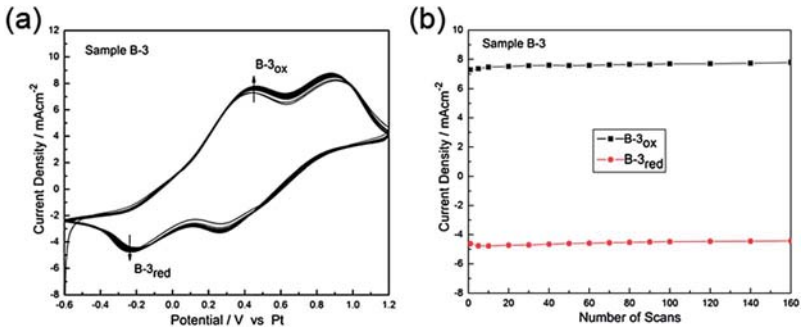

Fig. 6 Consecutive 160 CVs (a) of the I^-/I_3^- system for B-3 PANI CE at a scan rate of 100 mV s^{-1}, the relationship (b) between the number of scans and the resultant redox peak currents from (a).

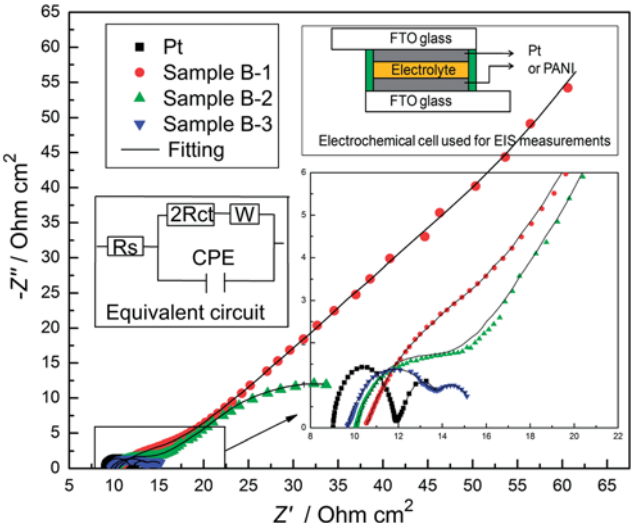

Fig. 7 Nyquist plots of the symmetrical Pt, B-1, B-2 and B-3 PANI CEs, respectively.

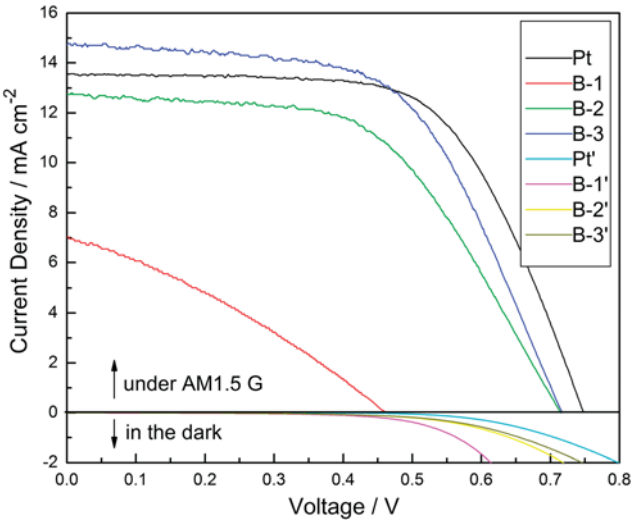

Fig. 8 Photocurrent density–voltage characteristics of DSSCs based on the Pt, B-1, B-2 and B-3 PANI CEs, respectively.

Table 3 The photovoltaic parameters of DSSCs with Pt, B-1, B-2 and B-3 PANI CEs, respectively

Samples	J_{SC}/mA cm^{-2}	V_{OC}/V	FF	η (%)
Pt	13.58 ± 0.05	0.75 ± 0.05	0.63 ± 0.04	6.39 ± 0.05
B-1	7.02 ± 0.02	0.46 ± 0.03	0.32 ± 0.02	1.04 ± 0.02
B-2	12.75 ± 0.04	0.71 ± 0.04	0.55 ± 0.03	5.01 ± 0.04
B-3	14.70 ± 0.04	0.72 ± 0.04	0.59 ± 0.03	6.21 ± 0.04

comparable to those of a cell with a Pt CE (9.06 and 1.48 Ω cm^2, respectively).[42,47,49]

Conclusions

In summary, an enhanced electrocatalytic activity for the PANI CE was demonstrated by means of a two-step CV approach, under a potential range firstly set between 0 V and 1.3 V for 1 cycle for the first-step pre-electropolymerization and then subjected to the second-step for PANI electropolymerization between 0 V and 0.8 V for 10 cycles *vs.* Ag/AgCl at a scan rate of 0.05 V s^{-1}. In the case of the two-step CV method, a small quantity of PANI as a function of crystal nucleus in the crystal growth was pre-electropolymerized under a suitably high potential at the first-step, then subjected to the second-step for PANI electropolymerization at a low potential for small number of scans. It can be noted that well-controlled and short-branched PANI nanofibers with high performance could be electropolymerized quickly when the electropolymerization method was switched from the one-step mode to the two-step mode. The two-step PANI CE showed improved excellent electrocatalytic activity for the I_3^-/I^- redox reaction compared to the conventional one-step PANI CE due to its higher cathodic peak current in CV tests and a lower R_{ct} value. The enhancement in the electrocatalytic activity can be attributed to the increased active surface area from its well-controlled and short-branched surface morphology. The low-cost DSSC using the two-step PANI CE yielded a conversion efficiency of 6.21% under full sunlight illumination (100 mW cm^{-2}, AM1.5 G), which is up to ~97% of that using the Pt CE. The present work suggests that the two-step PANI CE shows great potential as a cost-effective CE alternative for Pt-free DSSCs.

Acknowledgements

The authors appreciate funding from National Natural Science Foundation of China (21274082 and 21073115) and Shanxi province (2012021021-3), the Program for New Century Excellent Talents in University (NCET-10-0926) and the Scientific Research Start-up Funds of Shanxi University (020351801003).

References

1 B. O' Regan and M. Grätzel, *Nature*, 1991, **353**, 737.
2 L. Han, A. Islam, H. Chen, C. Malapaka, B. Chiranjeevi, S. Zhang, X. Yang and M. Yanagida, *Energy Environ. Sci.*, 2012, **5**, 6057.
3 J. Burschka, N. Pellet, S. Moon, R. Humphry-Baker, P. Gao, M. Nazeeruddin and M. Grätzel, *Nature*, 2013, **499**, 316.
4 M. Grätzel, *Nature*, 2001, **414**, 338.
5 A. Hagfeldt, G. Boschloo, L. Sun, L. Kloo and H. Pettersson, *Chem. Rev.*, 2010, **110**, 6595.
6 E. Olsen, G. Hagen and S. Lindquist, *Sol. Energy Mater. Sol. Cells*, 2000, **63**, 267.
7 J. Wu, Y. Xiao, G. Yue, Q. Tang, J. Lin, M. Huang, Y. Huang, L. Fan, Z. Lan, S. Yin and T. Sato, *Adv. Mater.*, 2012, **24**, 1884.
8 Y. Xiao, J. Wu, G. Yue, J. Lin, M. Huang, Z. Lan and L. Fan, *Electrochim. Acta*, 2012, **85**, 432.
9 S. Huang, L. Li, Z. Yang, L. Zhang, H. Saiyin, T. Chen and H. Peng, *Adv. Mater.*, 2011, **23**, 4707.
10 Z. Yang, T. Chen, R. He, G. Guan, H. Li, L. Qiu and H. Peng, *Adv. Mater.*, 2011, **23**, 5636.
11 H. Choi, H. Kim, S. Hwang, W. Choi and M. Jeon, *Sol. Energy Mater. Sol. Cells*, 2011, **95**, 323.
12 T. Chen, L. Qiu, Z. Yang, Z. Cai, J. Ren, H. Li, H. Lin, X. Sun and H. Peng, *Angew. Chem., Int. Ed.*, 2012, **51**, 11977.
13 H. Sun, D. Qin, S. Huang, X. Guo, D. Li, Y. Luo and Q. Meng, *Energy Environ. Sci.*, 2011, **4**, 2630.
14 Y. Xiao, J. Wu, J. Lin, S. Tai and G. Yue, *J. Mater. Chem. A*, 2013, **1**, 1289.
15 Y. Xiao, J. Wu, J. Lin, G. Yue, J. Lin, M. Huang, Y. Huang, Z. Lan and L. Fan, *J. Mater. Chem. A*, 2013, **1**, 13885.
16 G. Li, J. Song, G. Pan and X. Gao, *Energy Environ. Sci.*, 2011, **4**, 1680.
17 M. Wu, Q. Zhang, J. Xiao, C. Ma, X. Lin, C. Miao, Y. He, Y. Gao, A. Hagfeldt and T. Ma, *J. Mater. Chem.*, 2011, **21**, 10761.
18 Q. Li, J. Wu, Q. Tang, Z. Lan, P. Li and J. Lin, *Electrochem. Commun.*, 2008, **10**, 1299.
19 J. Wu, Q. Li, L. Fan, Z. Lan, J. Lin, P. Li, M. Huang and S. Hao, *J. Power Sources*, 2008, **181**, 172.
20 Y. Xiao, J. Lin, S. Tai, S. Chou, G. Yue and J. Wu, *J. Mater. Chem.*, 2012, **22**, 19919.
21 Q. Tang, H. Cai, S. Yuan and X. Wang, *J. Mater. Chem. A*, 2013, **1**, 317.
22 Q. Li, H. Chen, L. Lin, P. Li, Y. Qin, M. Li, B. He, L. Chu and Q. Tang, *J. Mater. Chem. A*, 2013, **1**, 5326.
23 Q. Li, X. Chen, Q. Tang, H. Xu, B. He and Y. Qin, *J. Mater. Chem. A*, 2013, **1**, 8055.
24 Y. Xiao, J. Wu, J. Lin, G. Yue, J. Lin, M. Huang, Z. Lan and L. Fan, *J. Power Sources*, 2013, **241**, 373.
25 Q. Li, X. Chen, Q. Tang, H. Cai, Y. Qin, B. He, M. Li, S. Jin and Z. Liu, *J. Power Sources*, 2014, **248**, 923.
26 X. Zhao, J. Zang, Y. Zang, Y. Wang, L. Bian and J. Yu, *Electrochem. Commun.*, 2009, **11**, 1297.
27 J. Zhang, T. Hreid, X. Li, W. Guo, L. Wang, X. Shi, H. Su and Z. Yuan, *Electrochim. Acta*, 2010, **55**, 3664.
28 L. Hung, Z. Wang, H. Wang, X. Cheng, A. Mitra and Y. Yan, *J. Mater. Chem.*, 2002, **12**, 388.
29 K. Huang, J. Huang, C. Wu, C. Liu, H. Chen, C. Chu, J. Lin, C. Lin and K. Ho, *J. Mater. Chem.*, 2011, **21**, 10384.
30 Z. Li, B. Ye, X. Hu, X. Ma, X. Zhang and Y. Deng, *Electrochem. Commun.*, 2009, **11**, 1768.
31 H. Karami, M. G. Asadi and M. Mansoori, *Electrochim. Acta*, 2012, **61**, 154.
32 Y. Xiao, J. Lin, J. Wu, S. Tai and G. Yue, *J. Power Sources*, 2013, **233**, 320.
33 Y. Xiao, J. Wu, G. Yue, J. Lin, M. Huang and Z. Lan, *Electrochim. Acta*, 2011, **56**, 8545.
34 J. Lin, J. Liao and S. Chou, *Electrochim. Acta*, 2011, **56**, 8818.
35 J. Wu, Z. Lan, J. M. Lin, M. Huang, S. Hao, T. Sato and S. Yin, *Adv. Mater.*, 2007, **19**, 4006.
36 M. Grätzel, *Progr. Photovolt.: Res. Appl.*, 2000, **8**, 171.
37 G. Wang, W. Xing and S. Zhuo, *Electrochim. Acta*, 2012, **66**, 151.
38 X. Mei, S. Cho, B. Fan and J. Ouyang, *Nanotechnology*, 2010, **21**, 395202.
39 Z. Huang, X. Liu, K. Li, D. Li, H. Luo, H. Li, W. Song, L. Chen and Q. Meng, *Electrochem. Commun.*, 2007, **9**, 596.
40 Y. Saito, W. Kubo, T. Kitamura, Y. Wada and S. Yanagida, *J. Photochem. Photobiol., A*, 2004, **164**, 153.
41 S. Biallozor and A. Kupniewska, *Electrochem. Commun.*, 2000, **2**, 480.
42 J. Lin and J. Liao, *J. Electrochem. Soc.*, 2012, **159**, D65.
43 H. Guo, Y. Li, L. Fan, X. Wu and M. Guo, *Electrochim. Acta*, 2006, **51**, 6230.
44 X. Wu, H. Ma, S. Chen, Z. Xu and A. Sui, *J. Electrochem. Soc.*, 1999, **146**, 1847.
45 A. Fujiwara, Y. Matsuoka, Y. Matsuoka, H. Suematsu, N. Ogawa, K. Miyano, H. Kataura, Y. Maniwa, S. Suzuki and Y. Achiba, *Carbon*, 2004, **42**, 919.
46 S. Moriyama, K. Toratani, D. Tsuya, M. Suzuki, Y. Aoyagi and K. Ishibashi, *Phys. E.*, 2004, **24**, 46.
47 G. Mor, K. Shankar, M. Paulose, O. Varghese and C. Grimes, *Nano Lett.*, 2006, **6**, 215.
48 M. Nazeeruddin, A. Kay, I. Rodicio, R. Humphry-Baker, E. Mueller, P. Liska, N. Vlachopoulos and M. Graetzel, *J. Am. Chem. Soc.*, 1993, **115**, 6382.
49 E. Ramasamy, W. Lee, D. Lee and J. Song, *J. Power Sources*, 2007, **165**, 446.

